

## Effect of Capillary Action on Short Term Electrochemical Corrosion Behaviour of X70 Steel in Unsaturated Saline Soil

Jianjian Wei<sup>1</sup>, Bin He<sup>1,\*</sup>, Yongxiang Feng<sup>1</sup>, Junlong Xu<sup>1</sup>, Dengqin Liang<sup>1</sup>, Lifeng Hou<sup>2</sup>, Pengju Han<sup>1</sup>, Xiaohong Bai<sup>1</sup>

<sup>1</sup> College of Civil Engineering, Taiyuan University of Technology, Taiyuan, 030024, China

<sup>2</sup> College of Materials Science and Engineering, Taiyuan University of Technology, Taiyuan, 030024, China

\*E-mail: [hebin@tyut.edu.cn](mailto:hebin@tyut.edu.cn)

Received: 7 May 2022 / Accepted: 20 June 2022 / Published: 7 August 2022

---

In this study, electrochemical impedance spectroscopy (EIS) was used to analyse the short-term corrosion of X70 steel in four soil corrosion systems with different NaCl content affected by capillary water. The results showed that the short-term electrochemical corrosion behaviour of X70 steel in saline soil was significantly affected by capillary water. In a soil corrosion system with NaCl content of less than or equal to 1.0%, the polarization resistance  $R_p$  of X70 steel at position 1# was generally less than that at position 2#, and the corrosion rate of X70 steel at position 1# was greater. SEM results showed that the degree of corrosion pit ulcer on the surface of X70 steel at position 1# was generally greater than that at position 2# in the soil with a NaCl content less than or equal to 1.0%. In addition, the equivalent circuits of X70 steel at positions 1#, 2# were  $R_s(C_1R_1(WR_{ct}Q))$  and  $R_s(WR_{ct}Q)$ , respectively, by fitting the EIS results. The impact of the capillary water upturn on the corrosion of X70 steel was further determined by analysing the equivalent circuit parameters and EDS results.

---

**Keywords:** Electrochemical impedance spectroscopy (EIS); Polarization curve; X70 steel; capillary water

### 1. INTRODUCTION

It has been nearly 20 years since the first-line project of the West to East gas transmission project was completed and put into operation. With the continuous advancement of natural gas transmission from West to East projects, high-strength buried pipeline steel has been manufactured and used in great quantities [1]. However, due to long-term embedment, metal is eroded by the soil medium, resulting in surface corrosion, strength reduction and other damage, that is, metal soil corrosion [2-4]. The corrosion of buried metals has restricted the pace of human infrastructure construction. The main types of surface damage caused by buried metals are electrochemical corrosion of soil and stray current corrosion. As an

effective detection method, electrochemical detection is widely used in the study of metal corrosion [5-8]. Many scholars at home and abroad have carried out research on this topic. The influencing factors affecting the corrosion status of buried metals, such as salt content [9, 10], temperature [11, 12], pH [13], microorganisms [14] and other action mechanisms, have been gradually developed and improved. Zhang et al. [15] studied the influence of simulated soil solution on the electrochemical behaviour of X70 pipeline steel by using orthogonal detection and strong dynamic polarization measurement and concluded that X70 steel has a lower corrosion degree in a low temperature, low oxygen content and weakly acidic environment. Bai et al. [16] analysed the factors influencing the kinetics of the corrosion behaviour of X80 steel. It was found that chloride ions have a strong adsorption capacity in positive temperature environments, which contributes significantly to the occurrence of corrosion. Based on the theory of electrochemical impedance spectroscopy, He et al. [17-19] systematically analysed and studied the corrosivity of sodium chloride-contaminated sand and its electrochemical corrosion behaviour on X70 steel under different influencing factors, especially under the condition of soil particle size change. You et al. [20] studied the corrosion behaviour of soil by electrochemical measurement, scanning electron microscopy and X-ray diffraction. The results showed that the corrosion rate is directly proportional to the content of water and salt, and the conductivity of pore water in the corrosion system is mainly water. With increasing chloride concentration, more corrosion products are generated, which hinders the transmission of oxygen. The above representative research results have contributed greatly to the development and improvement of buried metal corrosion theory. However, there is no relevant research on the effect of capillary action on the corrosion behaviour of buried pipeline steel in unsaturated saline soil.

In this study, the short-term electrochemical corrosion behaviour of X70 pipeline steel in different buried depths of saline soil was studied by EIS, SEM and EDS. Two equivalent circuit models are proposed for X70 steel at two positions with different degrees of influence by capillary water rise, and the solid-liquid-gas three-phase change model and conductive path characteristics during capillary water rise are constructed. This allows us to improve our understanding of the effect of capillary water rise on the electrochemical impedance of X70 steel and is important for further exploration of its corrosion mechanism.

## 2. MATERIALS AND EXPERIMENTS

### 2.1. Test material preparation

The soil used for the test was taken from Taiyuan, Shanxi Province, China, at a sampling depth of 1.5 m. After the test soil samples were retrieved, the soil particle size distribution curves were obtained by indoor tests, as shown in Figure 1. The X-ray diffraction (XRD) results of the soil samples are shown in Figure 2. In addition, the basic physical and chemical properties of the soil obtained by the liquid-plastic combine tester and DDSJ-307A tester are listed in Table 1. The retrieved test soil was crushed and dried by natural air and then screened for 2 mm for standby. After a certain amount of NaCl (analytical grade) was dissolved in deionized water, and the NaCl solution was fully stirred and mixed

with the standby soil. Finally, saline soil with NaCl content of 0.3%, 1.0% and 3.0% was obtained. At the same time, the soil with 0% NaCl content was configured as a reference. After the soil samples were prepared, they were placed into a constant-temperature and -humidity box and allowed to stand for 24 hours. The mass moisture content of the soil samples was controlled at 12.24%.

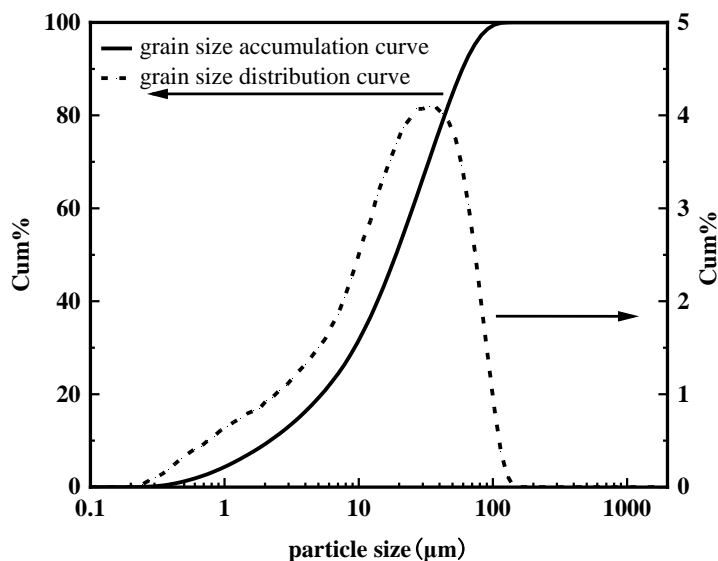


Figure 1. Soil particle size distribution

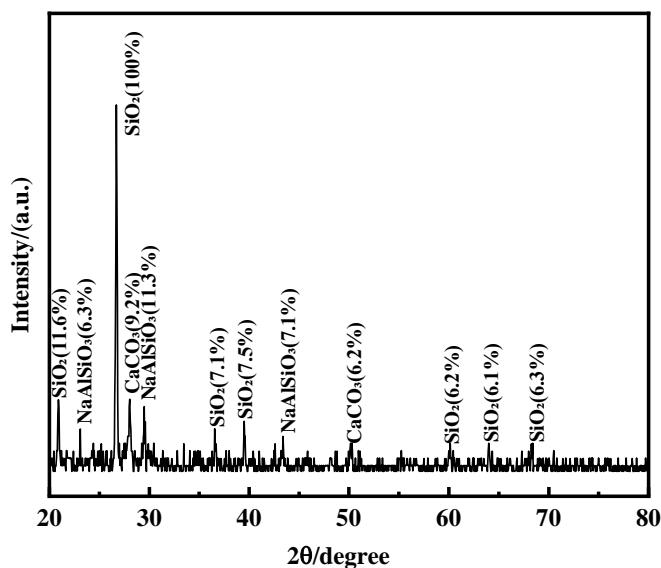


Figure 2. XRD analysis of test soil samples

Table 1. Basic physical and chemical properties of soil

parameters	natural water content (%)	liquid limit (%)	plastic limit (%)	plastic index	pH
values	12.24	30.30	18.80	11.50	7.2

The pipeline steel used in this test was X70 pipeline steel used in the West to East Gas Transmission Line 1 project. The main chemical composition of X70 steel is the average value obtained by analysing and testing three groups of samples, and the relevant parameters are listed in Table 2. In this test, the size of the X70 steel sample was 15 mm × 15 mm × 2 mm. X70 steel samples were polished one by one with 800-1500 mesh sandpaper on a grinder, polished with 2000 mesh sandpaper, and finally ultrasonically cleaned in deionized water. To facilitate electrochemical measurements, copper conductors were soldered to X70 steel. Additionally, a 10 mm × 10 mm working surface was left on the X70 steel surface and covered with epoxy resin.

**Table 2.** Main chemical composition of X70 pipeline steel (wt.%)

C	Si	Mn	P	Cr	Ni	Mo	Cu	Co	V	S	Fe
0.0645	0.201	1.906	0.0119	0.021	0.021	0.234	0.012	0.013	0.011	<0.0005	Balance

## 2.2. Test device

Geo-experts one dimensional (1D) soil column instrument and CS350 electrochemical workstation were used in this test. A schematic diagram of the device is shown in Figure 3. Geo-experts 1D soil column instrument is composed of a constant water supply system, plexiglass cylinder, ML2x moisture sensor and DL6 monitoring storage equipment. The plexiglass body has a height of 700 mm, outer diameter of 300 mm and inner diameter of 280 mm. The bottom of the plexiglass cylinder is connected to a constant water supply system to simulate the rising process of capillary water. The positions 120 mm and 570 mm away from the bottom of the barrel are named positions 1# and 2#, respectively. An ML2x moisture sensor was arranged to monitor the change in volume moisture content at these two positions during the test.

A CS350 electrochemical workstation was used in this test. The electrochemical test adopts a three-electrode system. X70 steel was used as the working electrode (WE), a platinum electrode was used as the counter electrode (CE), and a saturated calomel electrode was used as the reference electrode (RE). Three soil columns were made for each corrosion system with different salt content, the measurement was repeated 3 times, and a representative result was taken.

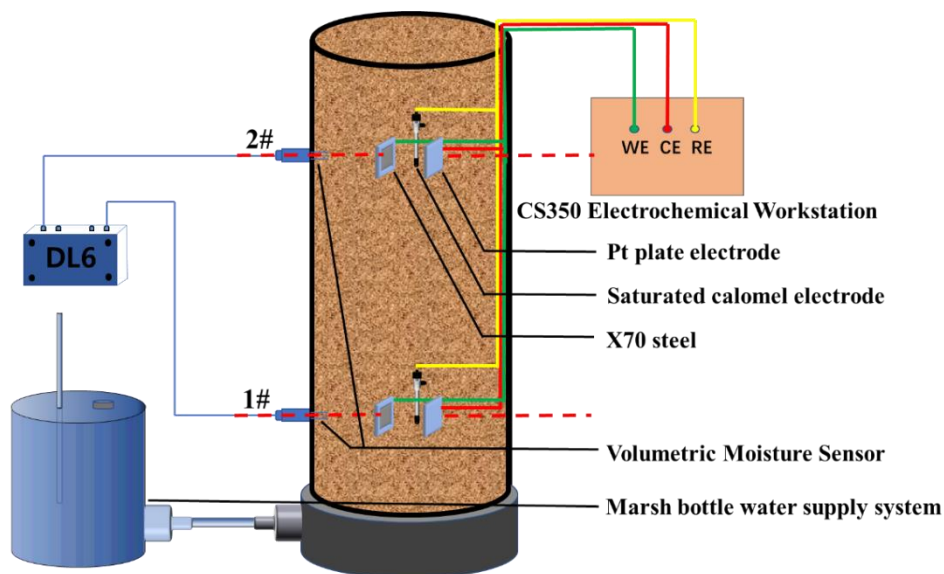


**Figure 3.** Schematic diagram of test device

### 2.3. Test process

First, Vaseline was applied to the inner wall of the plexiglass cylinder to reduce the boundary effect. A uniform layer of Vaseline on the inner wall of the plexiglass cylinder could make the inner wall of the plexiglass cylinder smooth, which was expected to effectively prevent water channels between the inner wall of the plexiglass cylinder and the soil pores. Then, the plexiglass cylinder was fixed on the test base. Finally, the prepared soil sample that was standing in the constant temperature and humidity box was removed for 24 hours and placed into the one-dimensional soil column instrument for layered compaction. Specifically, a certain mass of soil was weighed at a time and compacted by a manual compaction method to a thickness of 1 cm. The purpose was to maintain the same density throughout the column. This process was repeated to complete the compaction of the entire soil column while the X70 steel sheet and electrodes were buried at specific locations. The X70 steel and electrodes required for the electrochemical test were arranged at plexiglass cylinder positions 1# and 2#. A waterproof and breathable film was arranged on the top of the plexiglass can body to prevent water loss. The flow of the test soil column with buried samples and the electrode arrangement is shown in Figure 4.

In this test, an ML2x moisture sensor was used to monitor the change process of the volume moisture content at soil column positions 1# and 2# within 7 days. At the same time, an electrochemical test of X70 steel was carried out with a CS350 electrochemical workstation at the age of 7 days. The CS350 was switched on for 30 minutes to allow the potential to stabilize prior to electrochemical testing. The measurement frequency range of EIS was  $10^{-1} \sim 10^5$  Hz, the sweep frequency mode adopted the linear logarithmic sweep method, and the applied sine wave amplitude was 10 mV. The sweep range for the polarisation curve was -0.75 to 3 V at a scanning frequency of 2 mV/s. In addition, the corrosion products of X70 steel after 7 days of corrosion were observed by SEM, and the element composition was analysed.

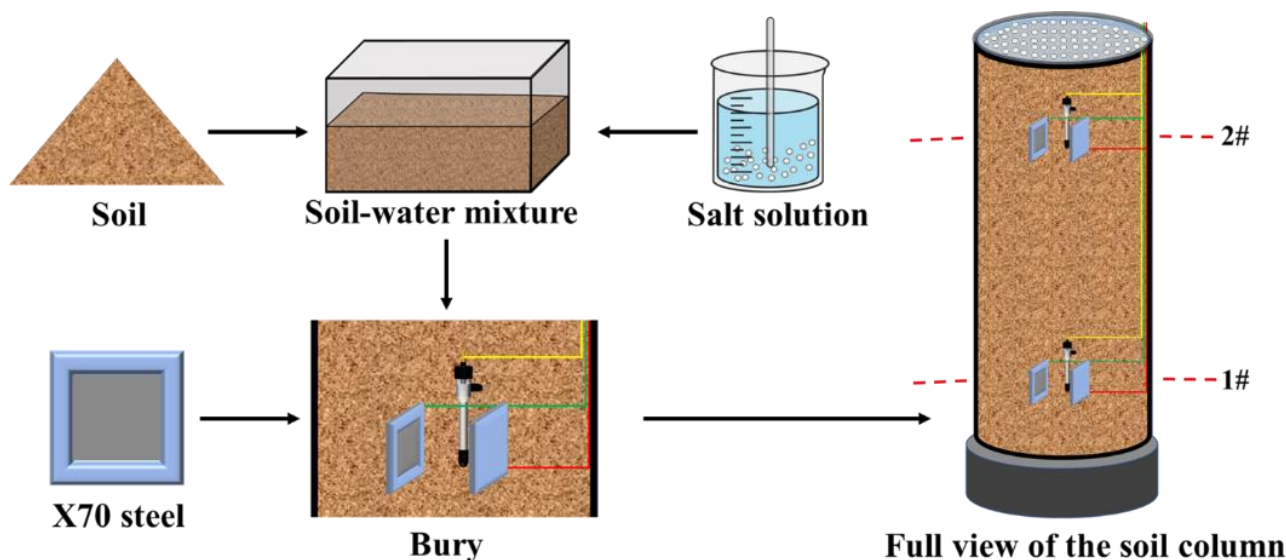


Figure 4. Experimental flowchart

### 3. RESULTS AND ANALYSIS

#### 3.1. Polarization curve measurement

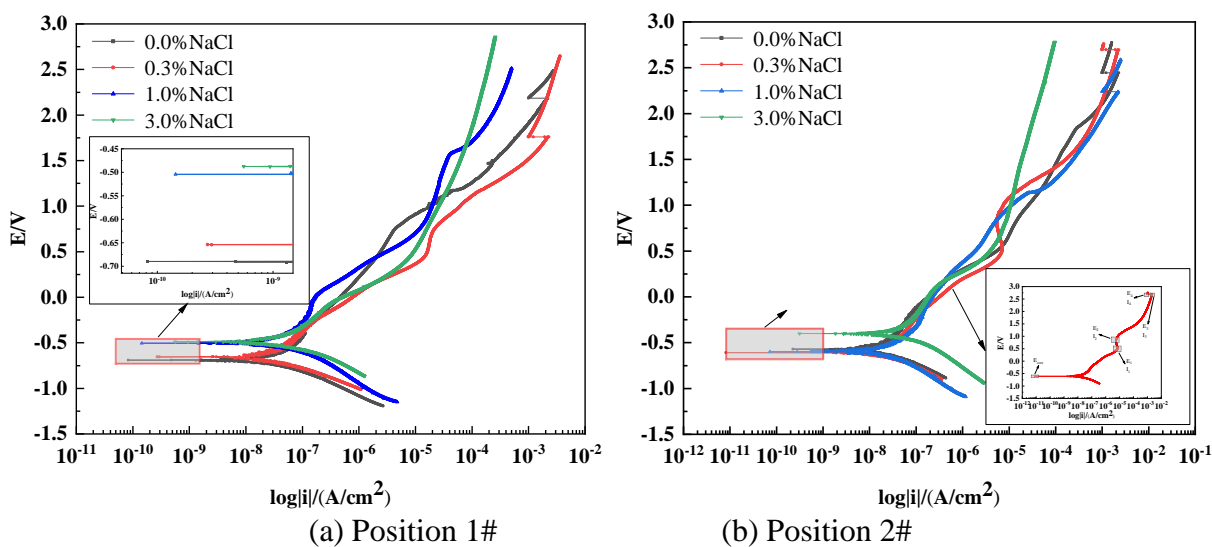


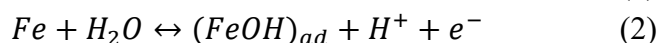
Figure 5. Polarization curves of X70 steel after 7 days for positions 1# and 2# in corrosion system

The polarization curves of the X70 steel buried in saline soil with NaCl content of 0.0%, 0.3%, 1.0% and 3.0% for 7 days are shown in Figure 5. Figure 5(a) shows the polarization curve of X70 steel at position 1#, and Figure 5(b) shows the polarization curve of X70 steel at position 2#. Figure 5 shows that the polarization curves of the X70 steel at positions 1# and 2# in the corrosion system with NaCl content of 0.0% and 0.3% show metal passivation. This might be related to the self-passivating metal element Cr in the chemistry of the X70 steel selected for this test. Cr is often added to Fe to improve the

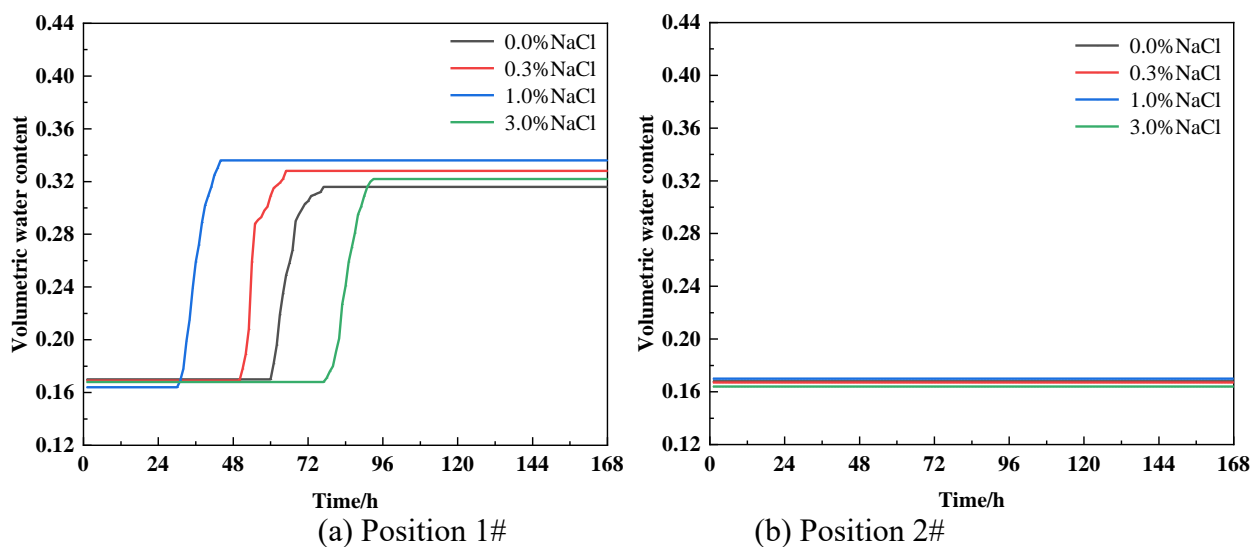
oxygen resistance of Fe. Under passivation conditions, the corrosion potential of the metal was located in the passive potential region, and the corrosion rate of the metal depended on the chemical dissolution rate of the passive film on the surface of X70 steel. The passivation of metal was due to the formation of a very thin and dense protective film with good coverage on the metal surface when the metal acts with a corrosive medium [21]. Due to the presence of this protective film, the metal substrate was mechanically separated from the corrosion medium. This hindered the exchange of material between the metal matrix and the corrosion system, resulting in a decrease in the dissolution rate of the metal and the metal moving from an activated to a passive state [22]. When there were active ions such as  $\text{Cl}^-$  in the corrosion system, it was easier than other ions to penetrate the original pores or defects in the film under the action of diffusion or an electric field. The interaction between  $\text{Cl}^-$  and the metal formed soluble compounds and promoted the corrosion reaction. In addition, there were many clay particles in the test soil. When there was NaCl in the soil corrosion system,  $\text{Na}^+$  replaced the original  $\text{Al}^{3+}$  and  $\text{Mg}^{2+}$  plasma in the electric double layer on the surface of the soil clay particles, which increased the thickness of the clay electric double layer and the dispersion degree of the clay colloid [23]. At this time,  $\text{Cl}^-$  in the corrosion system was easier to disperse in the oxide film to form a colloidal state. This doping could significantly change the electronic and ionic conductivity of the oxide film and destroy the protective effect of the film. Comparing the polarization curves in the soil corrosion system with a NaCl content of 1.0% in both figures in Fig. 5(a)(b), it can be clearly observed that passivation occurred in X70 steel at position 2# but not at position 1#. This difference should be attributed to the effect of the capillary water rise. As a result of the rise of capillary water, position 1# in the soil corrosion system with 1.0% NaCl at 7 days was located below the wetting front of capillary water, while position 2# was located above the wetting front. This caused two locations 1# and 2# of the soil corrosion system to have differences in water content. The wetting front below the soil corrosion system in the soil capillary pores was almost all occupied by water, and the corrosion system in the pore water was interconnected. This was more conducive to the transfer of  $\text{Cl}^-$  ions in the soil corrosion system. The moisture content above the wetting front was relatively low, and the pore water in the soil was easily locked in the narrow pores between soil particles. At this time, ion exchange in the system was more difficult.

Figure 5(b) shows that secondary passivation occurred for X70 steel at position 2# in the soil corrosion system with a NaCl content of 0.3%. We can clearly observe four characteristic points in the anodic polarization curves of such areas where metal passivation occurs [24]. In the  $E_{\text{corr}}$  (-0.606 V) to  $E_1$  (0.476 V) range, we generally consider that the metal is in a state of active dissolution. At this time, the X70 steel surface mainly occurs in the dissolution of metal (Equation 1) when the corrosion behaviour is in line with Tafel's law. When the potential continues rising to  $E_1$ , the X70 steel surface generates a thin and dense passivation film, and passivation of X70 steel occurs. The passivation potential is  $E_1 = 0.476$  V, and passivation current density  $I_1 = 6.781 \times 10^{-6}$  A/cm<sup>2</sup>. When the potential continues to rise to  $E_2 = 0.890$  V, the current density decreases to  $I_2 = 5.807 \times 10^{-6}$  A/cm<sup>2</sup>, at which time  $E_2$  is called the fade potential [25]. The cause of the passivation phenomenon at this point can be attributed to the generation of transitional oxides that change the surface state (Equation 2). Subsequently, the potential increased from  $E_2 = 0.890$  V to  $E_3 = 2.694$  V. During this period, the relationship between the current and potential can be regarded as a linear relationship, and the current density increases with increasing potential. Finally, the potential increased from  $E_3$  to  $E_4$ , and the potential change ( $\Delta E = E_4 -$

$E_3 = 0.004 \text{ V}$ ) was small, but the current density decreased significantly. This indicates that X70 steel has secondary passivation, and  $E_4$  is called the over passivation potential. Potential is a very important characteristic parameter in the study of metal corrosion. In addition to its application in corrosion kinetics, it is widely used in other aspects to assist in the study of metal corrosion. The electrochemical corrosion tendency of metals can be judged by their self-corrosion potential. Figure 5(a) shows that the self-corrosion potential of X70 steel at position 1# for 7 days moves positively toward the coordinate axis as the NaCl content in the corrosion system increases, and the thermodynamic trend of corrosion decreases. However, the self-corrosion potential of X70 steel at position 2# shows a negative shift followed by a positive shift law. The corrosion thermodynamic trend first increases and then decreases.



To more visually represent the effect of the capillary water rise, the variation curves of the volumetric water content at 1# and 2# in the soil corrosion system with different NaCl content over a 7-day period are shown in Figure 6. From Figure 6, we know that location 1# in all four soil corrosion systems with different NaCl content was already located below the capillary water wetting front at 7 days. As shown in Fig. 6 (a), the volume moisture content of the soil corrosion system with four different levels of NaCl content at location 1# increased and finally stabilized. Moreover, the rising rate of capillary water first accelerated and then slowed down with increasing NaCl content. The reasons for this phenomenon are well understood. When the content of NaCl in the soil corrosion system was 0.3% and 1.0%, the NaCl dissolved in water increased the rising rate of capillary water because it improved the surface tension of the soil particles. When the content of NaCl in the soil increased to 3.0%, the presence of sodium chloride in the water increased its specific gravity and thickness of the water film on the surface of the particles. This increased the blocking effect of capillary water rising and slowed down the rising speed of capillary water. In addition, Figure 6(b) shows that the volume moisture content did not change significantly within 7 days. This shows that position 2# of the four soil corrosion systems was above the capillary water wetting front.



**Figure 6.** Volumetric water content variation curves for positions 1# and 2# in corrosion system over 7-day period

To further quantitatively describe the corrosion condition of X70 steel in the corrosion system at 7 days, the electrochemical corrosion parameters of X70 steel were obtained by fitting the polarization curves using CView2 software in this paper and are listed in Table 3. As seen from Table 3, except for the soil corrosion system with a NaCl content of 3.0%, the polarization resistance  $R_p$  of X70 steel at position 1# is generally lower than that of X70 steel at position 2# in the same NaCl content soil corrosion system. The cause of this phenomenon can be attributed to the rise of capillary water. The pores of the soil particles at position 1# were occupied by pore water. This led to a decrease in the polarization resistance [26]. The polarization resistance is often inversely proportional to the corrosion rate [27]. Therefore, it can be inferred that the corrosion rate of the X70 steel at position 1# is higher than that at position 2# in the soil corrosion system with the same NaCl content except for the soil corrosion system with 3.0% NaCl content. The corrosion current density  $I_{\text{corr}}$  and corrosion rate fitted in Table 3 further verify this inference. In addition, it can be seen from Table 3 that the  $I_{\text{corr}}$  and corrosion rate of X70 steel at position 1# show a tendency to increase with increasing NaCl content. The  $I_{\text{corr}}$  and corrosion rate of X70 steel at position 2# showed a trend of decreasing and then increasing with increasing NaCl content. The reason why the  $I_{\text{corr}}$  and corrosion rate of X70 steel at position 2# of the soil with 0.3% NaCl decreased by one order of magnitude might be due to the secondary passivation of this X70 steel.

**Table 2.** Electrochemical corrosion parameters of X70 steel

Position	Salt content (%)	Ba (mV/dec)	Bc (mV/dec)	$R_p$ ( $\Omega/\text{cm}^2$ )	$I_{\text{corr}}$ ( $\text{A}/\text{cm}^2$ )	$E_{\text{corr}}$ (V)	Corrosion Rate (mm/a)
1#	0.0%	114	107	$1.91 \times 10^6$	$1.06 \times 10^{-8}$	-0.689	$1.35 \times 10^{-4}$
	0.3%	105	124	$1.43 \times 10^6$	$1.26 \times 10^{-8}$	-0.653	$1.49 \times 10^{-4}$
	1.0%	200	140	$1.39 \times 10^6$	$2.19 \times 10^{-8}$	-0.499	$2.57 \times 10^{-4}$
	3.0%	310	172	$1.30 \times 10^6$	$3.54 \times 10^{-8}$	-0.485	$4.16 \times 10^{-4}$
2#	0.0%	138	146	$1.94 \times 10^6$	$1.11 \times 10^{-8}$	-0.574	$1.30 \times 10^{-4}$
	0.3%	149	118	$2.43 \times 10^6$	$7.49 \times 10^{-9}$	-0.606	$8.80 \times 10^{-5}$
	1.0%	249	219	$1.40 \times 10^6$	$2.06 \times 10^{-8}$	-0.596	$2.43 \times 10^{-4}$
	3.0%	573	242	$1.00 \times 10^6$	$7.35 \times 10^{-8}$	-0.399	$8.64 \times 10^{-3}$

## 3.2. Electrochemical impedance spectroscopy measurement

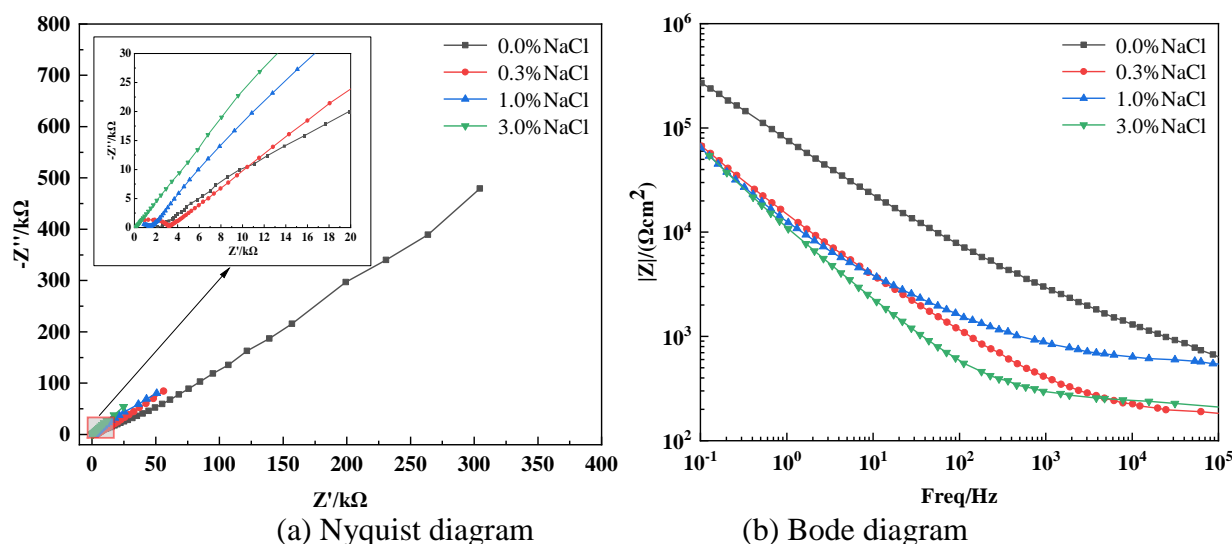


**Figure 7.** Nyquist and Bode diagram of X70 steel at position 1# in corrosion system after 7 days

The Nyquist and Bode diagrams of X70 steel at position 1# in the saline soil corrosion system at 7 days are shown in Figure 7. Figure 7 shows that 1# in the Nyquist diagram of X70 steel at 7 days is composed of a small capacitive reactance arc in the high-frequency region, large capacitive reactance arc in the medium-frequency region and diffusion tail arc in the low-frequency region. Compared with the soil corrosion system without NaCl and with a NaCl content of 0.3%, the intersection of the high-frequency region capacitive resistance arc and the real axis in the Nyquist plot of X70 steel in the soil corrosion system with NaCl content of 1.0% and 3.0% shifts to the left. This indicated that as the NaCl content in the soil corrosion system increased, the pore solution resistance at position 1# decreased significantly. This provided great convenience for current and ion transport in the corrosion regime. We can easily draw the same conclusion from the Bode plot of the X70 steel at position 1# at 7 days. The Bode plot reflected the relationship between impedance and frequency, where the impedance value decreased with increasing frequency, often reaching the highest value of impedance at the low-frequency extremes. Generally, the higher the impedance modulus in the low-frequency region, the better the corrosion resistance of the metal and the less likely the metal was to be corroded [28]. From the Bode plot in Figure 7, we can clearly see that the impedance modulus of X70 steel in the soil corrosion system containing NaCl is significantly lower than that of X70 steel in the soil corrosion system without NaCl. This indicated that an increase in NaCl significantly improved the corrosion capacity of the soil corrosion system.

To describe in more depth the electrochemical impedance characteristics of the X70 steel at position 1# in the corrosion system at 7 days, we applied the electrochemical equivalent circuit model. The electrochemical equivalent circuit model is shown in Figure 8, and the relevant fitted parameters obtained by applying ZView2 software are listed in Table 4. In the equivalent circuit model,  $R_s$  represents the soil resistance,  $R_1$  represents the transfer resistance of the clay particles to the pore solution, and  $C_1$  represents the clay bilayer capacitance. In addition,  $R_{ct}$  represents the charge transfer resistance, and  $W$

represents the Weber impedance Warburg. The capacitance C of the corrosion products generated on the surface of X70 steel is replaced by the constant phase angle element Q. The two parameters CPE-T and CPE-P of Q represent the ability of the bilayer capacitance to store charge and the similarity of the constant phase angle element to the pure capacitance, respectively [22]. The CPE-T values increase with increasing NaCl content in the soil corrosion system. The CPE-P parameters of the four corrosion systems X70 steel in Table 4 at position 1# are greater than 0.5, indicating that the corrosion product oxide film is more inclined to characterize the capacitive properties at this time. The corrosion product capacitance was due to the oxide film generated on the surface of X70 steel adhering to the surface of the X70 steel substrate, which impeded the transfer between the Fe<sup>2+</sup> generated by the dissolution of the metal and the gap solution. However, Cl<sup>-</sup> exists in the soil corrosion system. Due to its strong physical adsorption characteristics, Cl<sup>-</sup> was adsorbed on the surface of X70 steel corrosion products to produce pitting corrosion on the oxide film. The soil resistance R<sub>s</sub> decreases with increasing NaCl content. This was because the electrical conductivity of saline soils was greater than that of nonsaline soils, and the electrical conductivity increased with increasing salt concentration [29]. Due to the increase in electrical conductivity, the soil resistance R<sub>s</sub> decreased, and the corrosiveness of the soil increased. The transfer resistance R<sub>1</sub> between the clay particles and the pore solution in Table 4 did not show a clear pattern. In contrast, the clay bilayer capacitance C<sub>1</sub> shows a clear pattern: the clay bilayer capacitance C<sub>1</sub> decreases with increasing NaCl content in the soil. The decrease in C<sub>1</sub> might be due to the increase in the electric double layer thickness [30]. The Al<sup>3+</sup> in the clay lattice was often partially replaced by Mg<sup>2+</sup> and Ca<sup>2+</sup> in the soil, thus making the clay lattice negatively charged. To maintain electrical neutrality, the clay surface was bound to adsorb some positive ions, which in turn left the surface because of hydration and formed a double electric layer. The thickness of the electric double layer of monovalent Na<sup>+</sup> was two times that of divalent Mg<sup>2+</sup> and Ca<sup>2+</sup>. With increasing NaCl content, the Na<sup>+</sup> concentration increased, the thickness of the clay double layer increased, and the capacitance of the clay double layer decreased. The charge transfer resistance R<sub>ct</sub> decreased with increasing NaCl content in the soil. The charge transfer resistance R<sub>ct</sub> was inversely proportional to the corrosion rate of the metal. Therefore, it was concluded that the corrosion rate of X70 steel at position 1# in the corrosion system increased with increasing NaCl content, which was consistent with the analysis of the polarization curve.

The total impedance of the equivalent circuit is

$$Z = R_s + \frac{1}{j\omega C_1 + \frac{1}{R_1 + \frac{1}{j\omega Q + \frac{1}{R_{ct} + (1-j)\frac{\sigma}{\sqrt{\omega}}}}}} \tag{3}$$

$$Z_Q = \frac{1}{Y_0} (j\omega)^{-n} \tag{4}$$

where Z is the total impedance. Q is the constant phase angle element, and Z<sub>Q</sub> is the impedance of the constant phase element. Y<sub>0</sub> and n are the parameters characterizing the equivalent elements of CPE, i.e. CPE-T and CPE-P, are frequency independent. n is a dimensionless exponent, which takes values in the range. When n = 0, CPE is equivalent to R. When n = 1, CPE is equivalent to C. j is the imaginary unit with  $j = \sqrt{-1}$ ; ω is the angular frequency with  $\omega=2\pi f$ , where f is the voltage signal frequency.

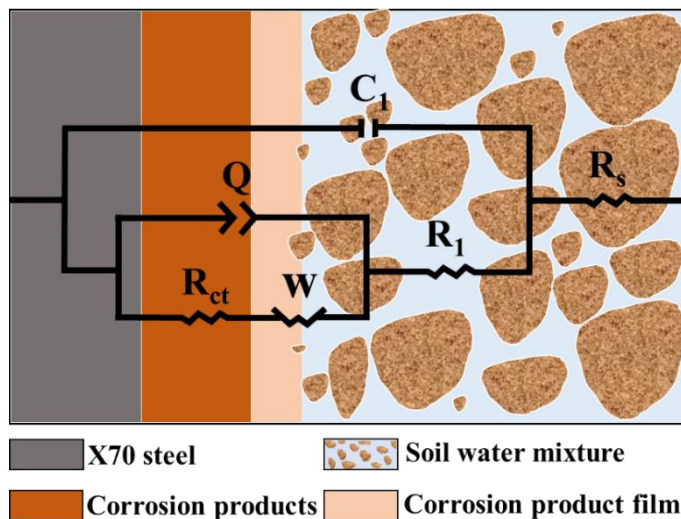


Figure 8. Equivalent circuit model of X70 steel at position 1# in corrosion system after 7 days

Table 4. Equivalent circuit parameters for X70 steel at position 1#

NaCl content	$R_s$ ( $\Omega/\text{cm}^2$ )	$R_1$ ( $\Omega/\text{cm}^2$ )	$C_1$ ( $\text{F}/\text{cm}^2$ )	$R_{ct}$ ( $\Omega/\text{cm}^2$ )	W1-R	W1-T	W1-P	CPE-T	CPE-P
0.0%	2284.00	763.20	$6.66 \times 10^{-7}$	76798.00	$2.55 \times 10^6$	4.529	0.62	$6.66 \times 10^{-9}$	0.65
0.3%	323.70	2813.00	$9.25 \times 10^{-8}$	5775.00	$5.96 \times 10^5$	31.14	0.65	$9.25 \times 10^{-10}$	0.60
1.0%	311.90	1040.00	$3.34 \times 10^{-9}$	3363.00	$1.66 \times 10^6$	1.45	0.85	$1.15 \times 10^{-9}$	0.65
3.0%	113.40	47.00	$1.15 \times 10^{-9}$	1528.30	$1.34 \times 10^6$	0.42	0.78	$3.34 \times 10^{-7}$	0.71

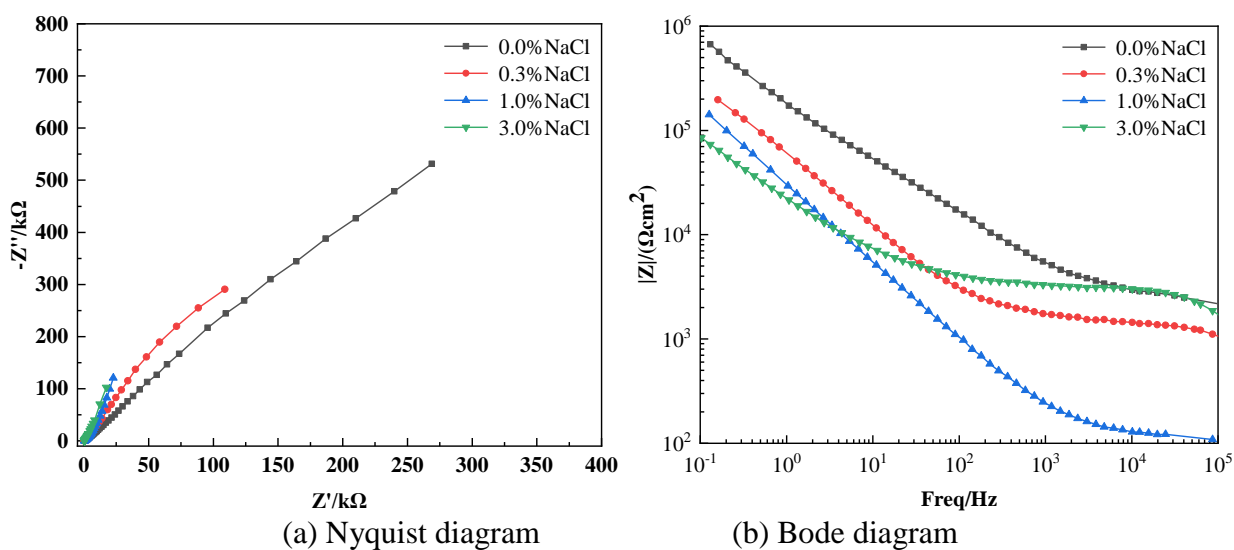


Figure 9. Nyquist and Bode diagrams of X70 steel at position 2# in corrosion system after 7 days

Nyquist and Bode plots of X70 steel at location 2# in the saline soil corrosion system containing

NaCl at 7 days are shown in Figure 9. Figure 9 shows that the Nyquist plot for X70 steel at position 2# has a large capacitive reactance arc that also exhibits a slightly diffuse Weber impedance. The Nyquist plot capacitive reactance arc in Figure 9 is significantly larger than that in Figure 7. This growth is more pronounced in saline soils containing NaCl. To describe in more depth the electrochemical characteristics of X70 steel at position 2#, we apply an electrochemical equivalent circuit model for illustration. The electrochemical equivalent circuit model is shown in Figure 10, and the relevant fitted parameters obtained by applying ZView2 software are listed in Table 5. In the equivalent circuit model in Figure 10, the actual physical meaning represented by each parameter is the same as in the equivalent circuit model in Figure 8. Unlike location 1#, the equivalent circuit model for location 2# does not add the transfer resistance  $R_1$  between the clay particles and the pore solution. Similarly, the clay bilayer capacitor  $C_1$  does not appear in the equivalent circuit. This indicates to some extent that the clay particles can only play a role at location 1#.

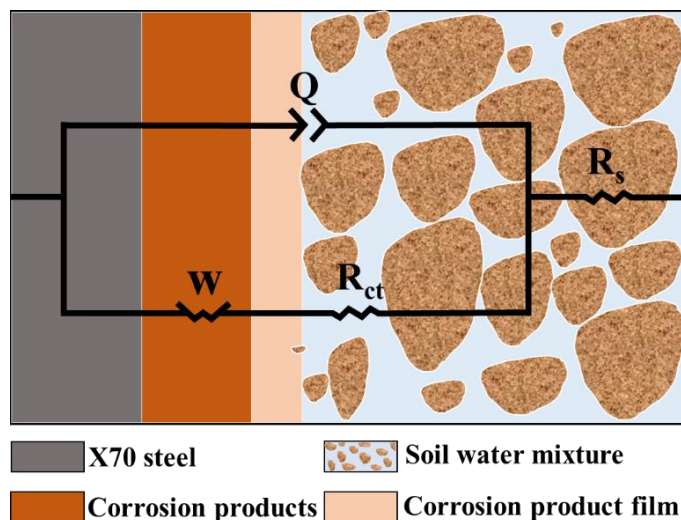
The reason for the different equivalent circuit models for the electrochemical corrosion behaviour of X70 steel at positions 1# and 2# of the soil column is obvious. Firstly, although locations 1# and 2# are in the same soil column, the rising capillary water makes the corrosive environment for the X70 steel at the two locations very different. Specifically, at 7 days location 1# was located below the capillary water wetting front and location 2# was located above the capillary water wetting front. Secondly, we can go on to analyse the reasons for the different equivalent circuit models used for locations 1# and 2#. Intuitively, the Nyquist diagram for the X70 steel at position #1, shown in Figure 7, has two capacitance arcs, which means that there are two time constants. Conversely, we can see in Figure 9 that the Nyquist diagram for X70 steel at position 2 has only one capacitance arc, which represents only one time constant. A deeper reason for this can be attributed to the difference in the effect of the short-term rise in capillary water on the corrosion of X70 steel at different locations. Position 1# has been in a high water content state (below the capillary water wetting front) for a long time, and in such an environment, the clay particles tend to play a more 'adhesive' role. This leads to a tighter bond between the corrosion products on the surface of the X70 steel and the clay particles. The formation of a double electric layer capacitance on the surface of the clay particles attached to the X70 steel-soil interface has an impact on the corrosion reaction of the X70 steel. Therefore, the clay double layer capacitance  $C_1$  and transfer resistance  $R_1$  between the clay particles and the pore solution are taken into account in the equivalent circuit model for the electrochemical corrosion of X70 steel at position 1#.

Table 5 shows that location 2# and location 1#, the soil resistance  $R_s$  shows the same law, and  $R_s$  decreases with increasing NaCl content. The charge transfer resistance  $R_{ct}$  with increasing NaCl content shows the law of increasing first and then decreasing. The increase in charge transfer resistance  $R_{ct}$  in the soil with a NaCl content of 0.3% was likely caused by the hindrance of ion transport by the corrosion product oxide layer. Note that the CPE-P parameter in the 0.3% NaCl soil corrosion system is less than 0.5, indicating that the X70 steel surface oxide film is more inclined to characterize the resistive properties at this time. The charge transfer resistance  $R_{ct}$  and CPE-P parameters in the 0.3% NaCl soil corrosion system both point to a lower transient corrosion rate of X70 steel at 7 days in the 0.3% NaCl corrosion system. This is consistent with the conclusions obtained from the polarization curves.

The total impedance of the equivalent circuit is

$$Z = R_s + \frac{1}{j\omega Q + \frac{1}{R_{ct} + (1-j)\frac{\sigma}{\sqrt{\omega}}}} \tag{5}$$

where the physical meaning of the relevant parameters is the same as in Equations 3 and 4.



**Figure 10.** Equivalent circuit model of X70 steel at position 2# in corrosion system after 7 days

**Table 5.** Equivalent circuit parameters for X70 steel at position 2#

NaCl content	$R_s$ ( $\Omega/\text{cm}^2$ )	$R_{ct}$ ( $\Omega/\text{cm}^2$ )	W1-R	W1-T	W1-P	CPE-T	CPE-P
0.0%	2837.40	79908.60	$1.83 \times 10^6$	68.12	0.51	$5.71 \times 10^{-6}$	0.58
0.3%	467.90	97156.30	$4.65 \times 10^5$	27.84	0.67	$2.51 \times 10^{-5}$	0.41
1.0%	321.90	3642.50	$2.34 \times 10^5$	4.30	0.72	$1.08 \times 10^{-5}$	0.62
3.0%	234.80	296.00	$1.31 \times 10^5$	4.62	0.73	$2.69 \times 10^{-5}$	0.68

### 3.3. Corrosion mechanism analysis

#### 3.3.1 Influence of capillary water rise on corrosion system mechanism

It has been pointed out that the ratio of the water content of the soil to the soil air content determines the type and intensity of corrosion [31]. The process of capillary water rise in unsaturated soils is in essence an increase in soil water content and a decrease in soil air content. The moisture content and the form in which it exists played a decisive role in the corrosion of metals in unsaturated soils [32]. The zoning of the corrosive environment of the soil affected by capillary water is shown in Figure 11. We named the part below the water table Area I. This area was not within the scope of our discussion. More important, we named the soil affected by capillary water action in a certain range above the water

table Areas II, III and IV, respectively. Among them, Area II is most seriously affected by capillary water. As the capillary water rises, the liquid phase occupies most of the pore channels between the soil particles at locations below the capillary water wetting front, and the connected liquid phase greatly facilitates ion transport in the corrosion regime. This contributes to a certain extent to the occurrence of corrosion [33]. At the same time, the location below the capillary water wetting front has an inhibiting effect on the cathodic reaction of the electrochemical reaction of the metal due to the formation of an oxygen-deficient environment. However, in the short term, this effect does not impede the corrosion of the metal to a great extent during the rise of the capillary water. Area III was also affected by the upturn of capillary water. As shown in Figure 11(c), an increase in water content enabled a continuous liquid level to be formed between soil particles in Area III and could also be connected with the atmosphere. This solid–liquid–gas three-phase state in Area III generally occurs at the location of the capillary water wetting front. In this case, the rate of the metal cathode reaction is often accelerated by the presence of the solid/liquid/gas triple phase boundary zone [34, 35]. In contrast, Area IV was least affected by capillary water. Figure 11(d) shows that the water in Area IV was adsorbed in the narrow channel between soil particles, so it was difficult to form a continuous liquid level. This hinders the transmission of ions in the corrosion system. This is consistent with the conclusions reached in most studies. When the water content is low, the void is only partly filled with water, and the surface area of the steel in contact with the electrolyte is even smaller, which results in a lower corrosion rate of the metal at this time [32, 36]. The ionization of iron into the soil is limited due to the low water content, making ion hydration incomplete [31]. The end result is that the corrosion rate of metals in this area is generally low.

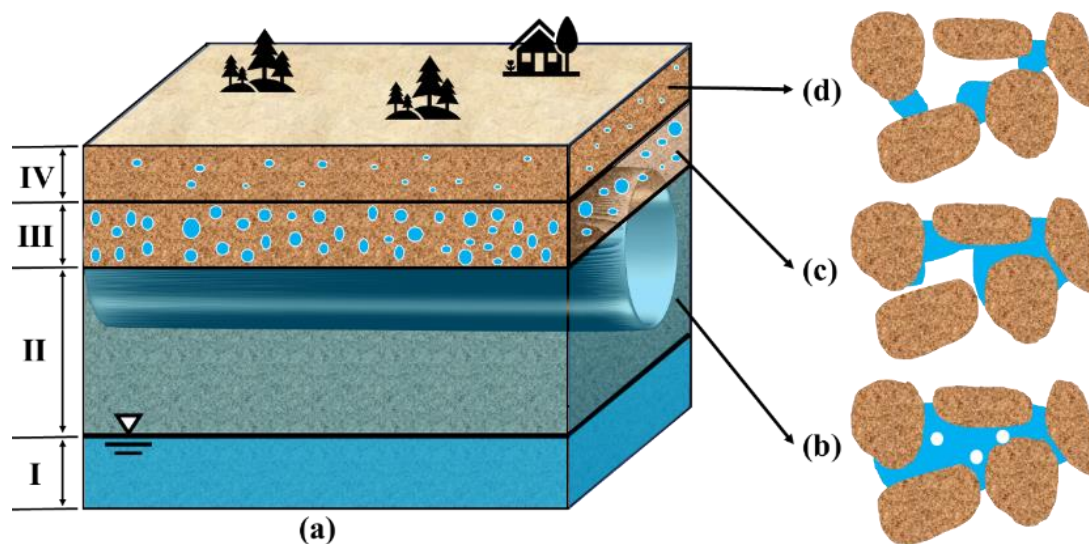


**Figure 11.** Three-phase solid–liquid–gas model of soil erosion system influenced by capillary action in unsaturated soil: (a) Zoning of soil corrosion systems by capillary action; (b) Area II; (c) Area III; (d) Area IV.

To further investigate the corrosion mechanism of X70 steel under capillary action in the short term, we showed the three-phase state of solid–liquid–gas and its conductive path in the soil corrosion system at locations 1# and 2# at 7 days in Figure 12. At 7 days, in the four soil corrosion systems with

different NaCl content used in this test, X70 steel at position 1# was below the capillary water wetting front, and X70 steel at position 2# was above the capillary water wetting front, as shown in Figure 12(a). According to the division of areas affected by capillary water mentioned above, we classified the soil corrosion system location 1# into Area II, and the current transmission path is shown in Figure 12(c). Similarly, we classified the soil corrosion system location 2# in Area IV and showed its current transfer path in Figure 12(b). In Figure 12(b), there are three conductive paths: aa, bb and cc. aa represents the conductive path passing only through soil particles, bb represents the conductive path passing through soil particle pore water air, and cc represents the conductive path passing through soil particle pore water. Three conductive paths are also present in Figure 12(c), a'a', b'b' and c'c' [37]. Among them, only c'c' is the most special, representing the conduction path that passes only through the pore solution. This conductive path is the most efficient. It is the presence of the c'c' conductive path that makes the charge transfer efficiency of the soil corrosion system at location 1# higher than that at location 2#. The reason for this can be attributed to the increased water content of the soil at location #1 due to capillary action, which makes the corrosion system more conductive at this location compared to location #2 [38, 39]. The final result is that in most cases, the corrosion rate of X70 steel at location #1 is generally greater than that at location #2. This was clearly demonstrated in the polarization curve fitting parameters section of this paper.

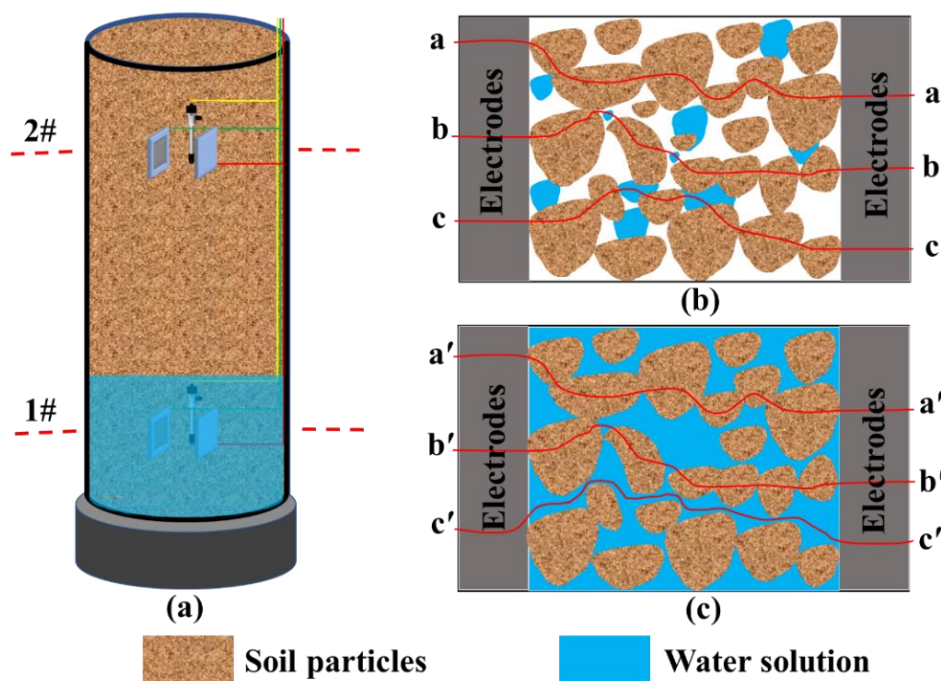


**Figure 12.** Three-phase morphology and conduction path in soil corrosion system under capillary water action: (a) Schematic diagram of three phases at different locations of soil corrosion system; (b) Conductive path between electrodes at position 2#; (c) Conductive path between electrodes at position 1#.

3.3.2 Micromorphological analysis

Microscopic images of X70 steel at 7 days in the saline soil corrosion system containing NaCl at locations 1# and 2# are shown in Figures 13 and 14, respectively.

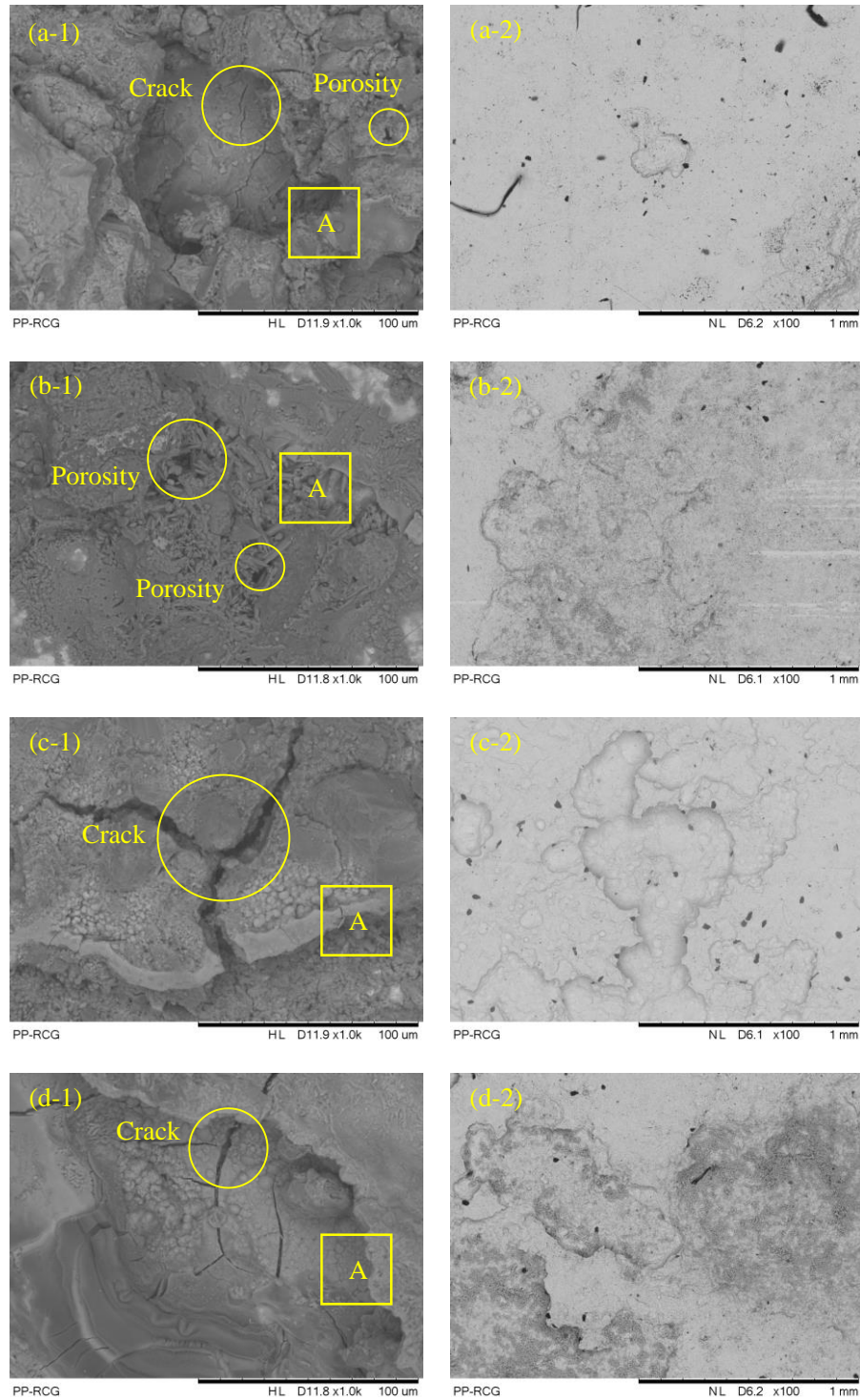


**Figure 13.** Microscopic images of X70 steel at position 1# in corrosion system after 7 days: (a) 0.0% NaCl; (b) 0.3% NaCl; (c) 1.0% NaCl; (d) 3.0% NaCl.

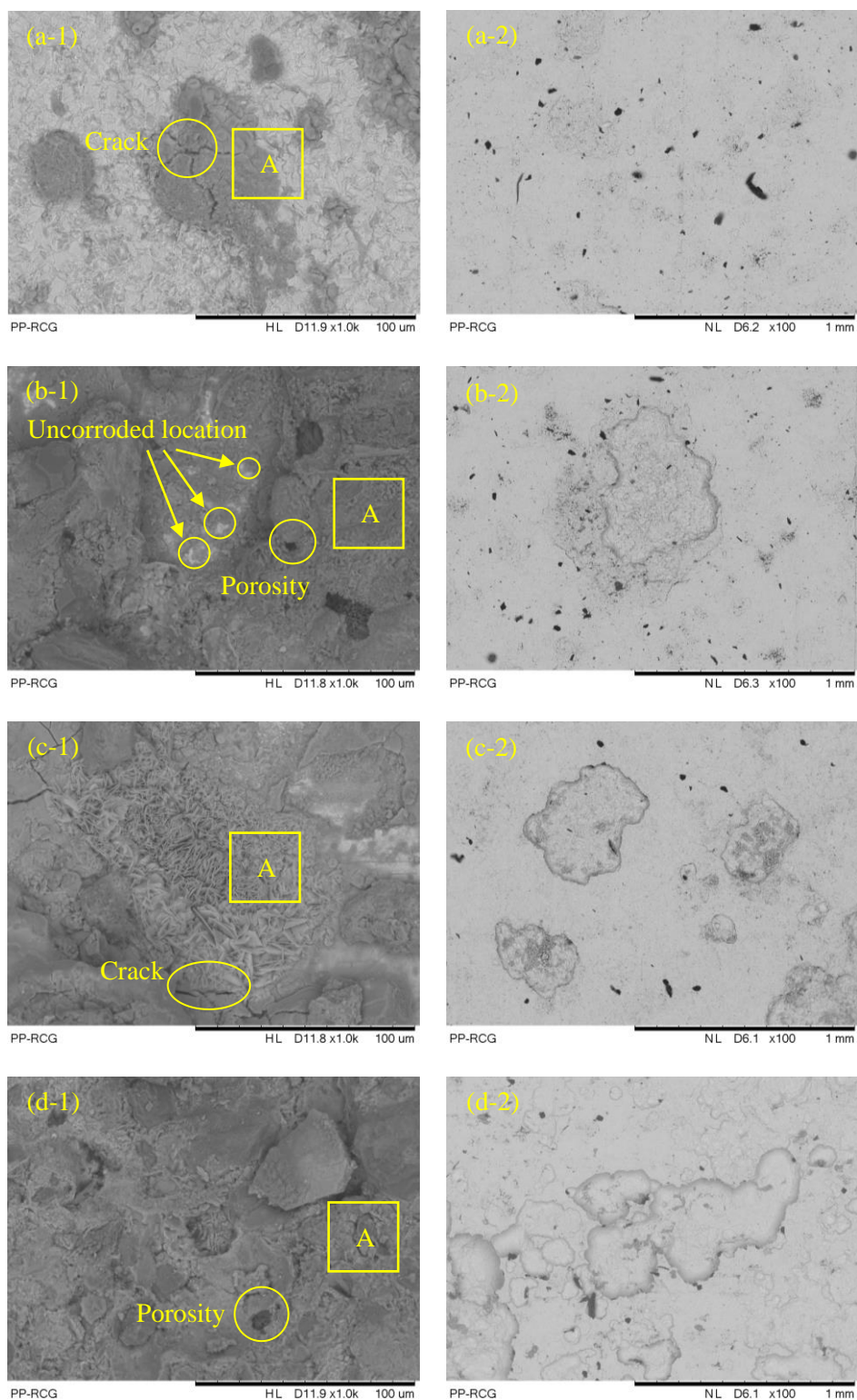
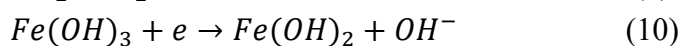
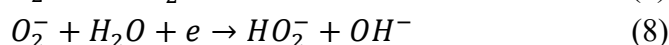


**Figure 14.** Microscopic images of X70 steel at position 2# in corrosion system after 7 days: (a) 0.0% NaCl; (b) 0.3% NaCl; (c) 1.0% NaCl; (d) 3.0% NaCl.

In the figure, the left side shows a microscopic image of the corrosion products on the surface of X70 steel magnified 1000 times, and the right side shows a microscopic image of the corrosion pit on

the surface of X70 steel magnified 100 times after the corrosion products are removed. As seen from Figures 13 and 14, cracks or damage points appeared on the surface of X70 steel at the soil corrosion system locations 1# and 2#. This was the main reason why the corrosion reaction of the X70 steel matrix continued to occur when it was wrapped by corrosion products. These corrosion products cover layer defects often occurred in the X70 steel surface of nonmetallic inclusions, porosity, certain impurities in the grain boundary of the deviations and other locations. These locations of ions easily penetrated the oxide film, and the metal surface easily adsorbed various ions from the surrounding media. With the formation of a passivation film, the corrosion reaction of the metal exhibited increased blockage [22]. When the oxidant played a role in the corrosion system to increase the corrosion potential of X70 steel and reach a certain critical value, aggressive  $Cl^-$  played an important role in the destruction of the passive film.  $Cl^-$  adsorbed to defects in the passivation film due to its physical adsorption properties and combined with cations in the passivation film to form soluble chlorides (Equation 6). This created active dissolution sites on the passivation film, which promoted the occurrence of metal pitting [40]. At the same time, the cathodic reaction of the metal (Equations 7, 8 and 9) occurred in addition to the reduction of oxygen but was also accompanied by the reduction of insoluble corrosion products (Equation 10). All of this further corroded the metal. By comparing the condition of corrosion pits on the surface of X70 steel in Figures 13 and 14, it can be seen that as the NaCl content increases, the number of corrosion pits increases and gradually develops into a large area of ulcers. In addition, we found that when the sodium chloride content was less than or equal to 1.0%, the collapse area of the corrosion pits of X70 steel in Figure 13 was generally larger than that in Figure 14. The rise in capillary water caused the water content at position 1# to be greater than that at position 2#. The change in water content might be the main reason for the difference in the ulcer area of X70 steel at these two positions [41, 42].



EDS scanning was carried out for the local range of area A in the figure, and the corresponding element analysis results were obtained and counted, as shown in Figure 15. Figure 15 shows that the main constituent elements of the X70 steel corrosion products at positions 1# and 2# in the saline soil corrosion system included Fe, O, Si, Ca and Al [43]. First, we found that the proportions of Fe and O were the highest. The proportion of Fe increased with increasing NaCl content, which could explain why the corrosion products also increased with increasing NaCl content to a certain extent. Second, it was not difficult to find that there are more Si and Ca elements in Figure 15(a), and the proportion was significantly higher than that in Figure 15(b). Both Si and Ca come from soil, which indicated that the content of soil in the corrosion products at position 1# was high. This was because the clay particles in position 1# were adsorbed on the surface of corrosion products and settled together with corrosion products. This further showed that clay particles played a role in position 1# below the capillary wetting front in the short term of the capillary rise. This was consistent with the conclusion obtained by electrochemical impedance. In addition, there was Al in the corrosion products, which might come from the sample stage.

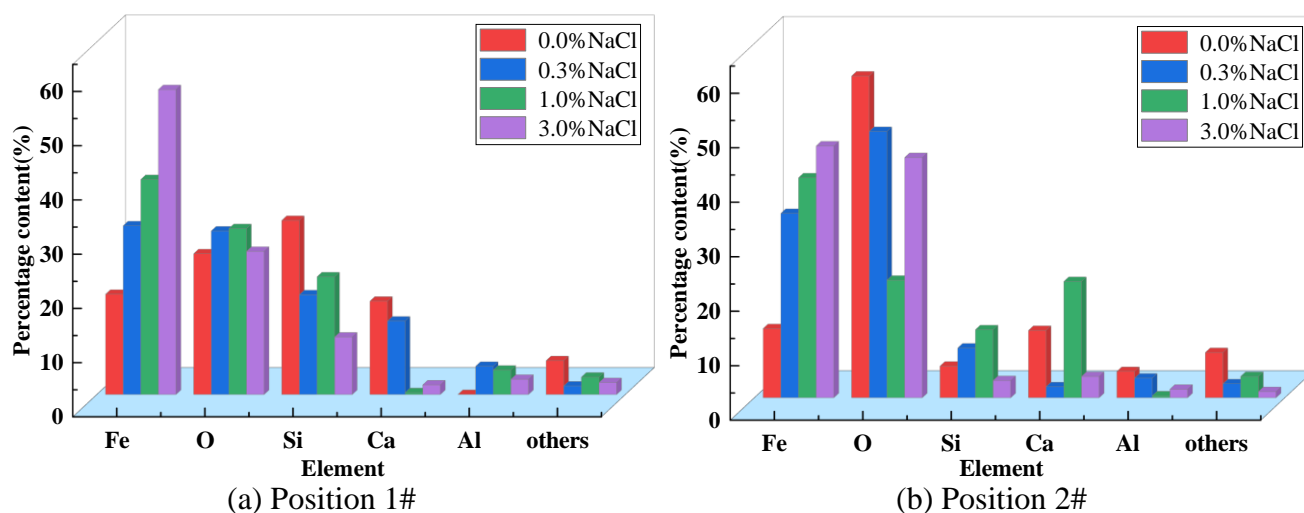


**Figure 15.** Elemental statistics of X70 steel corrosion products localized after 7 days in corrosion system at locations 1# and 2#.

#### 4. CONCLUSIONS

In this study, the short-term corrosion of X70 pipeline steel in saline soil under capillary action was investigated by EIS, SEM and EDS. The conclusions were as follows:

(1) The results of polarization curve analysis showed that the self-corrosion potential of X70 steel at position 1# increased with increasing NaCl content, and the thermodynamic trend of corrosion decreased and the corrosion rate increased. Influenced by a capillary water rise, the polarization resistance of X70 steel in the soil corrosion system with NaCl content less than or equal to 1.0% was generally lower at position 1# than at position 2#. The corrosion rate of X70 steel at position 1# was greater.

(2) The short-term electrochemical corrosion behaviour of X70 steel at two locations above and below the wetting front was significantly different due to the influence of rising capillary water. The equivalent circuit model for X70 steel at position 1# below the wetted front was  $R_s(C_1R_1(WR_{ct}Q))$ ; the equivalent circuit model for X70 steel at position 2# above the wetted front was  $R_s(WR_{ct}Q)$ . The reason for the difference in the equivalent circuit models at these two locations can be attributed to the adsorption of clay particles at location 1#.

(3) The results of microscopic image analysis showed that with an increase in NaCl content in the corrosion system, the quantity of corrosion pits on X70 steel at positions 1# and 2# increased and gradually developed into large-area ulcers. The degree of corrosion pit ulcer on X70 steel at position 1# was obviously greater than that at position 2# in the soil with a NaCl content less than or equal to 1.0%. In addition, EDS analysis results showed that the corrosion products of X70 steel increased with increasing NaCl content. Location 1# resulted in more Si and Ca elements in the corrosion products due to the adsorption of sticky particles. It was concluded that in the short-term corrosion of X70 steel, sticky particles played a great role below the wetting front.

## ACKNOWLEDGEMENTS

This work was funded by National Natural Science Foundation of China (Grant No. 41807256, 51178287), Applied Basic Research Program in Shanxi Province (Grant No. 20210302123139).

## References

1. Y. H. Li, H. Feng, Q. Chi, F. Fei, G. X. X. Gao, W. W. Li, X. F. Xu, H. Y. Chen and H. Zhang, *Math. Probl. Eng.*, 2021 (2021) 1.
2. M. N. Norhazilan, K. S. Lim, Y. Nordin and A. Abdullah, *Adv. Mater. Res.*, 311-313 (2011) 875.
3. W. Wang, D. Robert, A. Zhou and C. Q. Li, *J. Mater. Civ. Eng.*, 30 (2018) 04018272.
4. Y. Song, G. Jiang, Y. Chen, P. Zhao and Y. Tian, *Sci Rep*, 7 (2017) 6865.
5. H. Zhang, L. Yan, Y. Zhu, F. Ai, H. Li, Y. Li and Z. Jiang, *Metals*, 11 (2021) 1317.
6. D. H. Xia, C. Ma, S. Song, L. Ma, J. Wang, Z. Gao, C. Zhong and W. Hu, *Sens. Actuators, B*, 252 (2017) 353.
7. Y. Zhang, F. Huang, Q. Hu, Z. Peng and J. Liu, *Mater. Chem. Phys.*, 241 (2020) 122045.
8. Q. Hu, J. Liu, J. Zhang, F. Huang and X. P. Guo, *Adv. Mater. Res.*, 652-654 (2013) 1432.
9. I. M. Gadala and A. Alfantazi, *Corros. Sci.*, 82 (2014) 45.
10. X. Liu, Y. Tan, X. Zhang, Q. Liao and Z. Wang, *Corros. Rev.*, 38 (2020) 263.
11. I. B. Obot, I. B. Onyeachu, S. A. Umoren, M. A. Quraishi, A. A. Sorour, T. Chen, N. Aljeaban and Q. Wang, *J. Pet. Sci. Eng.*, 185 (2020) 106469.
12. L. Wang, *Int. J. Electrochem. Sci.*, 14 (2019) 161.
13. P. Han, *Int. J. Electrochem. Sci.*, 13 (2018) 8694.
14. Z. Zhou, T. Wu, M. Liu, B. Wang, C. Li and F. Yin, *Int. J. Pressure Vessels Piping*, 192 (2021) 104395.
15. L. Zhang, X. G. Li and C. W. Du, *J. Iron Steel Res. Int.*, 16 (2009) 52.
16. X. Bai, B. He, P. Han, R. Xie, F. Sun, Z. Chen, Y. Wang and X. Liu, *RSC Adv*, 12 (2021).
17. B. He, X. H. Bai, L. F. Hou, D. C. Zhang and P. J. Han, *Mater. Corros.*, 68 (2017) 846.
18. B. He, P. J. Han, L. F. Hou, C. H. Lu and X. H. Bai, *Mater. Corros.*, 67 (2016) 471.
19. B. He, C. H. Lu, P. J. Han and X. H. Bai, *Eng. Failure Anal.*, 59 (2016) 410.
20. Z. You, Y. Lai, H. Zeng and Y. Yang, *Constr. Build. Mater.*, 238 (2020) 117762.
21. Y. Lan, *Int. J. Electrochem. Sci.*, 16 (2021) ArticleID:210925.
22. F. Sun, *Int. J. Electrochem. Sci.*, 16 (2021) 150878.
23. M. Yan, C. Sun, J. Xu, J. Dong and W. Ke, *Corros. Sci.*, 80 (2014) 309.
24. L. S. Yang and C. Yang, *Pet. Sci.*, 18 (2020) 285.
25. Y. Y. Andreev, *Prot. Met. Phys. Chem. Surf.*, 45 (2009) 669.
26. Y. Guo, S. Xu and W. Shan, *Cold Reg. Sci. Technol.*, 151 (2018) 28.
27. B. He, P. Han, C. Lu and X. Bai, *Eng. Failure Anal.*, 58 (2015) 19.
28. A. Gangan, M. ElSabbagh, M. A. Bedair, H. M. Ahmed, M. El-Sabbah, S. M. El-Bahy and A. Fahmy, *Arabian J. Chem.*, 14 (2021) 103391.
29. X. Xu, W. Zhang and Y. Wang, *Acta Geotechnica*, (2022).
30. M. Özcan, İ. Dehri and M. Erbil, *Appl. Surf. Sci.*, 236 (2004) 155.
31. S. K. Gupta and B. K. Gupta, *Corros. Sci.*, 19 (1979) 171.
32. D. N. Dang, L. Lanarde, M. Jeannin, R. Sabot and P. Refait, *Electrochim. Acta*, 176 (2015) 1410.
33. J. Wei, B. He, Y. Feng, L. Hou, P. Han and X. Bai, *Mater.*, 15 (2022) 3426.
34. J. Jiang, J. Wang, Y. H. Lu and J. Z. Hu, *Electrochim. Acta.*, 54 (2009) 1426.
35. J. Wang, L. Liang and J. Jiang, *Electrochem. Commun.*, 10 (2008) 1788.
36. I. S. Cole and D. Marney, *Corros. Sci.*, 56 (2012) 5.
37. Z. Chen, *Int. J. Electrochem. Sci.*, 16 (2021) ArticleID:210914.
38. M. A. Malicki, R. Plagge and C. H. Roth, *Eur. J. Soil Sci.*, 47 (1996) 357.

39. O. H. Jacobsen and P. Schjonning, *J. Hydrol.*, 151 (1993) 147.
40. D. Sazou, A. Kominia and M. Pagitsas, *J. Solid State Electrochem.*, 18 (2013) 347.
41. A. Ismail and A. Elshamy, *Appl. Clay Sci.*, 42 (2009) 356.
42. J. K. Singh and D. D. N. Singh, *Corros. Sci.*, 56 (2012) 129.
43. X. Bai, B. He, P. Han, R. Xie, F. Sun, Z. Chen, X. Liu and Y. Wang, *J. Mater. Eng. Perform.*, 31 (2021) 968.

© 2022 The Authors. Published by ESG ([www.electrochemsci.org](http://www.electrochemsci.org)). This article is an open access article distributed under the terms and conditions of the Creative Commons Attribution license (<http://creativecommons.org/licenses/by/4.0/>).